Desalination and Water Treatment
www.deswater.com

doi: 10.5004/dwt.2022.28142

252 (2022) 50–65
March

Modification of poly(propylene fumarate) membrane by (graphene oxide/Pluronic F-68) additive: preparation, characterization and wastewater treatment

Ehsan Ghorban Nezhad, Ali Arastehnodeh*, Susan Khosroyar, Mahmoodreza Khadangi Mahrood

Department of Chemical engineering, Quchan branch, Islamic Azad University, Quchan, Iran, emails: aliarastehnodeh@iauq.ac.ir (A. Arastehnodeh), ehsan.ghorbannezhad1368@gmail.com (E.G. Nezhad), susankhosroyar@yahoo.com (S. Khosroyar), khadangi@iauq.ac.ir (M. Khadangi)

Received 14 March 2021; Accepted 29 November 2021

ABSTRACT

In this paper, novel flat sheet membranes were prepared via the vapor induced phase separation method and using the poly(propylene fumarate)/(graphene oxide/Pluronic F-68)/2-pyrrolidone casting solutions. The membrane properties such as morphology, mechanical, hydrophilicity and permeation properties were examined as functions of GO/Pluronic F-68 additive concentration and exposure vapor time. These membranes were characterized by scanning electron microscopy, Fourier-transform infrared spectroscopy, mechanical testing, molecular weight cut-off evaluation, contact angle measurement and dynamic wetting tests. The experimental results indicated that modified membranes exhibit significant differences in surface properties and inherent properties. Also, exposure time has an effective role in membrane structure. So that by increasing the exposure time up to 20 min, the structure of the membrane changed from an asymmetrical structure to a symmetrical structure with the cellular structure. In addition, an increase in mechanical properties and resistance of membranes was observed for the poly propylene fumarate membranes modified with GO/Pluronic F-68 and exposed to vapor for 20 min. These membranes have a relatively noticeable rejection of the local ceramic factory wastewater pollutants of properly than others.

Keywords: Vapor induced phase separation; Membrane; Poly(propylene fumarate); Graphene oxide; Pluronic F-68; Rejection

1. Introduction

Nowadays, there is a substantial emerging interest in fundamental and applied research on wastewater treatment using membrane filtration. There are different methods for membrane preparation such as phase separation, sol-gel process, stretching, interfacial reaction, track etching, microfabrication, etc. In these methods, phase separations are the most common method upon membrane fabrication [1].

Phase separation processes are mainly including non-solvent induced phase separation (NIPS), evaporation induced phase separation (EIPS), thermally induced phase separation (TIPS) and vapor-induced phase separation (VIPS) methods. The VIPS technique is a relatively slow process that allows a more uniform diffusion of vapor into the polymer, which offers better control in the phase inversion process [2]. In the VIPS, the cast film is exposed to an environment (typically open-air) with controlled humidity. The penetration of non-solvent into the film causes the polymer to precipitate, which results in the formation of a thin skin layer of a symmetric porous membrane [3].

* Corresponding author.

In the filtration industry, development of novel membranes with enhanced mechanical, permeation, anti-biofouling properties for membrane applications is of enormous importance [4]. Poly(propylene fumarate) (PPF) is a linear and unsaturated copolyester based on fumaric acid [5]. It has good mechanical performance, adjustable biodegradability, easy processing, etc. [6]. Despite these desirable properties, PPF has disadvantages. The main disadvantage of the PPF in membrane separation is related to the hydrophobicity property of it which leads to a low membrane flux and is easily susceptible to fouling. Therefore, efforts should be made to solve this problem by chemical or physical modifications. Several approaches that have been widely explored for membrane modification are include coating with hydrophilic materials [7,8], surface grafting polymerization [9], the addition of additives [10–12], coating with hydrophilic polymers [13–15] and so on.

Several critical hydrophilic materials explored for membrane modification, including single-walled carbon nanotubes (SWCNT), multi-walled carbon nanotubes (MWCNT), poly(ethylene glycol), graphene-based material and so on [16]. Among them, graphene-based materials have been considered for different fields of technology and science due to their unique properties, including excellent thermal properties, mechanical and chemical stability, high surface area, and low-cost production [17,18].

In recent years, graphene oxide (GO) has been considered the most common hydrophilic inorganic particle that is used for membranes modification. The presence of oxygenated functional groups such as hydroxyl, epoxy, and carboxyl in GO causes the modified membranes to have high effective flux and better antifouling properties [19]. Also, it takes pleasure in the high surface area, excellent mechanical and thermal stability, biocompatibility, prominent electron transport, cytotoxicity, and cost efficiency [20,21]. Additionally, the anti-bacterial property of GO would hinder straight contact among the bacterial cells and GO, which prevent bacteria growth [22,23].

It is one of the most well-known graphene derivatives which, has been recently applied in several fields such as in the biosensor preparation [24], biomedical applications [25], as well as additive for membranes applied in wastewater treatment [26,27].

One of the main problems associated with the preparation of membranes containing GO is possibly related to the more homogenous dispersion of GO into the polymer matrix. Graphene oxide having oxygen-containing functional groups can dissolve in polar solvents. So to improve the dispersion of it in organic solvents and better compatibility with polymer matrices, the GO must be modified by suitable agents [28]. One of the modification agents that can be used for GO dispersity in a nonpolar medium is Pluronic F-68. Pluronic F-68 is a nonionic triblock copolymer composed of a central chain of (poly(propylene oxide)) flanked by two hydrophilic chains of (poly(ethylene oxide)). The presence of a central hydrophobic chain of (poly(propylene oxide)) in Pluronic F-68 structure can improve the dispersion of graphene in nonpolar solutions [29]. So the presence of Pluronic F-68 into the membrane matrix is prominent in increasing the permeability and anti-fouling resistance and antibacterial properties for membrane applications.

The novelty in this research lies in introducing graphene oxide/Pluronic F-68 additive to the PPF to improve the performance of the PPF membrane for ceramic factory wastewater filtration. In order to improve the hydrophilic and morphological properties of PPF membrane, the graphene oxide that has been modified by Pluronic F-68 was added to the membrane. These membranes were prepared with the VIPS method. The effects of the modified additive concentrations and vapor exposure times on morphology, mechanical properties, hydrophilicity and permeation flux of the PPF membranes were investigated.

2. Experimental

2.1. Materials

Poly(propylene fumarate) (MW = 3,600 g/mol) was supplied from Merck (Germany). Solvent of 2-pyrrolidone with an analytical purity of 99% was supplied from Alfa Aesar (Germany). Pluronic F-68 (Molar mass = 1,000 g/mol; PEO weight content, %PEO = %70) (Molar mass of polypropylene glycol block: 850 g/mol, percentage of polyethylene glycol in molecule: 10%) was purchased from BASF. Graphene oxide (GO) was purchased from ACS Material LLC (Medford, MA).

PEG with an average molecular weight of 200 Da, 400 Da, 600 Da, 4 kDa, 20 kDa, 35 kDa, 100 kDa and 200 kDa were supplied from M/s, Sigma Chemicals. Dextran with average molecular weight of 70 kDa was purchased from Millipore Sigma Chemicals, USA. DI water was obtained by a purification system (Millipore). Wastewater used in the present study was supplied from a local ceramic factory. Three pollution indices of this wastewater, that is, turbidity, chemical oxygen demand (COD), and total dissolved solids (TDS), were in the range of 231 NTU, 2,131 mg/L, and 954 mg/L, respectively.

3. Methods

3.1. Non-covalent functionalization of GO

At first, GO and Pluronic F-68 were taken in a ratio of 1:3 in a 40 mL glass vial and then 10 mL of ultrapure water was added to dissolve Pluronic F-68. The mixture was sonicated by using an ultrasonic bath sonicator (PCI analytics) for 1 h at 60°C by vortexing the solution every 15 min. After that, the GO suspension was filtrated by vacuum filtration through a 0.22 μ nylon filter. The filtrate was centrifuged using ultracentrifuge (Sorvall Discovery M150 SE) for 6 h at 4°C, 23,000 rpm to remove the unbound Pluronic F-68. Then the GO/Pluronic F-68 solution is lyophilized, weighed out, dried and stored at −80°C.

3.2. Membrane preparation

For membrane preparation, at first the PPF was dissolved in a 2-pyrrolidone solvent with the concentration of 18%. The solution was stirred for one week to obtain a transparent and homogeneous solution. After that, the Pluronic F-68/GO additive was added, and the solution was treated in an ultrasonic bath for 30 min to complete dissolution and remove air bubbles to avoid membrane defects. After air

bubbles removed, an appropriate amount of polymer solution was cast on a glass plate with a 250 μm casting knife (casting speed of 2.5 m/min). The casting was carried out at a temperature of 25°C and humidity of 20%. For evaporation of the nascent membrane, the cast film was then placed in a closed cabin with a constant humidity of 80% at various exposure times (10, 20, 30 and 40 min), and then immersed in the coagulation bath with DI water for complete phase separation. After completing coagulation, the membranes were washed with ultra-pure water and then was transferred to distilled water overnight to wash out the rest of solvent.

3.3. Thermodynamic analysis

Ternary phase diagram was determined the diffusion rate of coagulant in the polymeric system and represented that whether or not a polymeric solution is suitable for membrane formation [30]. For this stabilization, cloud point measurement was done by the titration method. First, polymer solution with certain given content (wt.%) was taken into a glassware equipped with stirring. Then coagulant was slowly dropwise added from burette to the polymer solution until the local cloudy state occurred. By weighing of non-solvent, solvent and polymer present in the glassware, the ternary composition of cloud point can be obtained.

3.4. Membrane characterization

For investigation of membrane structure, scanning electron microscopy (SEM) images were made by using a FEI Quanta 200 ESEM (ThermoFisher Scientific, Waltham, MA, USA) under high vacuum and at a potential of 25 kV.

For this analysis, the membranes were immersed into liquid nitrogen and cross-section samples were prepared by creating smooth breaks of the frozen membranes using a razor blade. The samples were then coated with a thin film of conductive gold to minimize sample charging problems.

The bursting pressure to study mechanical stability was determined by using SANTAM 20KN testing machine at 25°C. At first, the membrane samples were placed with the skin-side facing down into the bursting pressure device. Then the plunger directly moved with a crosshead speed of 10 mm/min onto the sample. The bursting pressure of the device was raised continuously until it was reached to the extent that the pressure caused the membrane to break. Finally, the reached pressure was read from the meter of the device. An average of the reached pressures on three specimens was reported as a proper value.

The Fourier-transform infrared spectroscopy (FTIR, Thermo Nicolet iZ10, USA) spectroscopy was performed to analyze the membrane composition. Spectra represented correspond to the average of 16 scans captured at a resolution of 4 cm^{-1}.

For evaluation of membranes surface hydrophilicity, contact angle measurement was done by the technical equipment (JC2000D, Shanghai Zhongcheng Digital Technology Apparatus Co., Ltd., China).

Dynamic wetting tests were done by a Camtel CDCA-100F dynamic adsorption apparatus (Camtel, UK). The sample was cut to a size of 1 cm × 6 cm with sharp scissors. When the specimen was immersed to water, the weight of adsorbed water was detected and recorded. The dynamic water adsorption was plotted as a function of time.

Each membrane filtrate was analyzed for different pollution indices of turbidity, TDS and COD using turbidity DR/890 colorimeter (HACH), Myron L DS TDS Meter model 512T4 and YSI 910 COD colorimeter, respectively.

Molecular weight cut-off (MWCO) of the prepared membranes were determined by the rejection studies of different molecular weights of PEG (400 Da, 4 kDa, 6 kDa, 10 kDa, 20 kDa, 35 kDa, 100 kDa and 200 kDa) and also dextran 70 kDa. Solute rejection measurements were conducted in a stirred batch cell at 140 kPa pressure and 1,500 rpm. The permeate samples were analyzed using a refractometer (Abbe Refractometer Model 2WAJ, Australia). In this study, the molecular weight corresponding to 90% rejection was estimated as the MWCO of the membrane. The rejection values were plotted against the molecular weight of the solutes in a semi-logarithmic curve. The rejection was calculated using the following equation [31]:

$$R(\%) = \left(1 - \frac{C_p}{C_f}\right) \times 100 \tag{1}$$

where C_f and C_p are the concentration of solute in the feed and permeate, respectively.

The average pore radius of the membranes was achieved using Eq. (2) [32].

$$r_s = 16.73 \times 10^{-3} (\mathrm{MW})^{0.557} \tag{2}$$

where r_s is in nm and MW is in Da.

In order to measure the membrane porosity, the membrane sample with a certain dimension was dipped in water for 24 h. Then, the surface of the species was dried by filter paper and immediately weighed. After that, the membranes were dried in an oven at 50°C for 24 h and weighed again. Overall porosity (ε) was determined with the gravimetric method using the following equation [33]:

$$\varepsilon(\%) = \frac{W_w - W_d}{A \times l \times d_w} \times 100 \tag{3}$$

where W_w, W_d, A, l and d_w are wet and dry membrane weights (g), the surface area of membrane sample (cm^2), membrane thickness (cm) (measured by a digital micrometer (Mitotoyo, Japan)) and water density (0.998 g/cm^3), respectively.

3.5. Evaluation of membrane performance

To evaluation of the prepared membrane performance in ceramic factory wastewater filtration, batch cross-flow filtration was selected. The laboratory-scale membrane test unit that used in this research has mainly consisted of a feed tank, pump, and membrane module. Pure water flux (PWF) and rejection measuring were determined at a transmembrane pressure of 7 bar at ambient temperature. The retentate and permeate were returned to the feed tank in order to maintain constant concentration. Permeate flux was obtained from the volume of the permeate within 60

and 30 min for pure water and ceramic factory wastewater respectively and calculated as [34]:

$$J = \frac{m}{A \cdot \Delta t} \tag{4}$$

where J (L m^{-2}h) is the permeation flux, m (Kg) is the total weight of permeate in Δt (min) time, and A (m) is the membrane area. Membrane rejection (R) was measured at 7 bar according to Eq. (1) that C_p and C_f are the concentration of permeate and feed, respectively.

3.6. Preparation of the suspension culture of bacteria

Escherichia coli DH5α was taken on this research. First, LB medium was prepared by weighing the appropriate powder medium and adding to water in a sterile flask. Then the broth autoclave and cool to room temperature and consequently in a laminar flow chamber, transfer approximately 1 mL of overnight *E. coli* culture to the flask. Finally, seal the mouth of the flask with sterile cotton and incubate overnight at 37°C with continuous shaking.

3.7. Evaluation of anti-bacterial and anti-biofouling properties of membranes

The anti-bacterial property of modified membranes was evaluated as follows: after injection of *E. coli* bacteria to the suspension culture and incubation under constant agitation rate of 180 rpm for 10 h at 37°C, resulting suspension was diluted to about 107 (CFU)/mL by phosphate-buffered saline (PBS). The diluted suspension was pipetted into an agar plate and then exerted throughout the surface. The membrane samples that were cut (2 cm^2 × 2 cm^2), then placed on the agar surface and were incubated at 37°C for 24 h. After that, the plates were visually investigated for the bacteria colonies.

For investigation of the anti-biofouling property, the sterilized membranes were immersed in 10 mL bacterial suspension comprising 106 CFU/mL *E. coli* and incubated in the shaking incubator at 37°C for 12 h. After that, the membranes were removed from bacterial suspension and rinsed with DI water. SEM images were employed to study the surface of the unmodified and modified membranes. Moreover, the bacterial solutions were diluted with phosphate-buffered saline up to the concentration of 1 × 10^{-3} cell/mL. 1 mL of the diluted suspension was spread onto the surface of agar petri-dishes and incubated for 24 h at 35°C. The colonies were counted to estimate the number of viable *E. coli* remaining in the suspensions.

4. Results and discussion

4.1. Thermodynamic analysis

A ternary phase diagram can be present the thermodynamic states of the polymer solution. The phase separation in the VIPS process is based on the nucleation and growth mechanism and, or the spinodal decomposition mechanism. If the composition of the polymer solution locates in the meta-stable region, nucleation and growth mechanism occurs, resulting in a closed and cellular pore. A bi-continuous or a droplet morphology will form if the composition of the solution locates in the unstable region (spinodal decomposition mechanism). The ternary phase diagram of the (modified GO/PPF)/2-pyrrolidone/Vapor combination systems is obtained from the cloud points measurements which are shown in Fig. 1. As can be observed, the bimodal curve is shifted toward the modified polymer/solvent axis by increasing water concentration, which is even more noticeable the lower stability of the polymer solution. The hydrophilic nature of the Pluronic F-68 promotes water vapor inflow and causes lower thermodynamic stability.

4.2. Characterization

4.2.1. FTIR analysis

The FTIR spectrums of GO, Pluronic F-68, Pluronic F-68/GO, PPF and (Pluronic F-68/GO)/PPF membranes are shown in Fig. 2. In the FTIR spectra of GO, the strong and broad O–H stretching vibration band is evident at 3,410 cm^{-1}. Also, C=O stretching vibration band at 1,730 cm^{-1}, C–O stretching vibration at 1,087 cm^{-1} for the epoxy group, and O–H deformation vibration band at 1,404 cm^{-1} were observed. The Pluronic F-68 represents characteristic O–H stretching vibration at 3,433 cm^{-1}, C–H stretching vibration at ~2,886 cm^{-1}, and C–O stretching vibration at ~1,116 cm^{-1}. For PPF, the ester carbonyl bonds and C=C stretching appeared at 1,724 and 1,640 cm^{-1}, respectively. The FTIR of Pluronic F-68/GO exhibits characteristic peaks around 1,733 and 1,222 cm^{-1} ascribed to C=O and C–O, respectively. A specific peak appearing at 1,582 cm^{-1}, indicating the deformation of C–C bond due to the existence of epoxy groups. The spectrum of the (Pluronic F-68/GO)/PPF blending membrane exhibits bands at 3,530 cm^{-1} due to O–H stretching vibration, 1,654 cm^{-1} ascribed to the bonding vibration of C=C, and C=O in GO. The existence of oxygenized functional groups in (Pluronic F-68/GO)/PPF FTIR spectrum can be related to hydrogen interactions between the C=O groups of PPF and the –COOH groups of GO. Additionally, the characteristic peaks of Pluronic F-68 in blend membranes were overlapped by PPF peaks with the high relative intensity of the C–O bond appearing at 1,107 cm^{-1}.

4.2.2. SEM result

To evaluate the effect of GO/Pluronic F-68 and process parameters, including exposure time on the membrane structure, the SEM images were applied (Fig. 3). PPF is an amorphous polymer and SEM image of the neat PPF membrane show a finger-like structure.

SEM results of modified membranes with GO/Pluronic F-68 at exposure time of zero exhibit finger-like structure with a dense top-layer and porous sublayer. It is clear that by Pluronic F-68 loading to GO the finger-like pore size and the connectivity of the pores between the sub-layer and top-layer of the PPF membranes was changed.

The addition of GO/Pluronic F-68 causes a great diffusion velocity of water to the nascent membrane during the phase inversion, so macrovoids grow throughout the membrane. Homogeneous dispersion of the GO within the

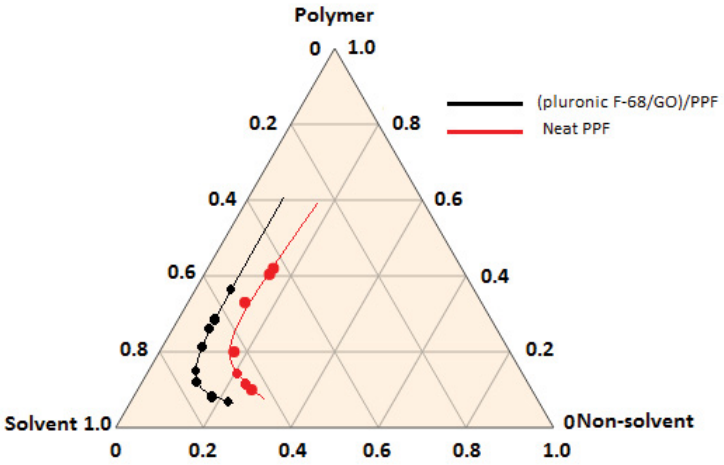

Fig. 1. Ternary phase diagram for modified PPF membrane prepared by VIPS process.

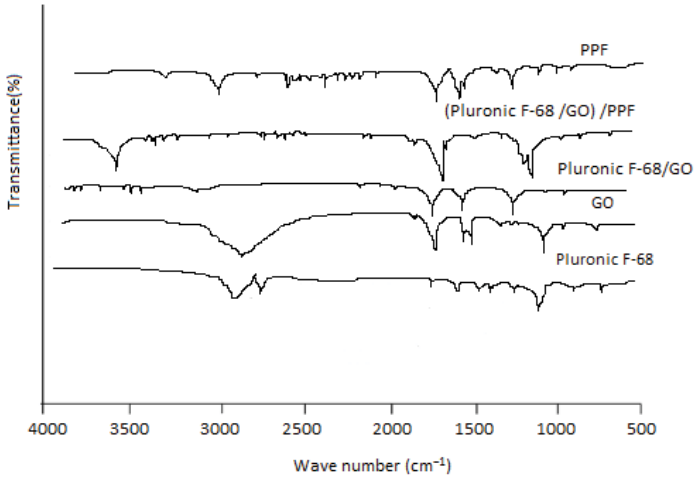

Fig. 2. FTIR spectra of Pluronic F-68, GO, Pluronic F-68/GO, PPF and membrane modified by Pluronic F-68/GO.

polymer matrix and preventing the aggregation of the GO by Pluronic F-68 loading, results in the more regular formation of macrovoids in the membrane. The micelle structure of the casting solution is mainly depends on the Pluronic F-68 presence on it. So that the density of the micelles influences the membrane structure. Results show that the size of micelles was increased by increasing GO/Pluronic F-68 up to 4 wt.% and consequently, the membranes with the macroporous support layer, dense skin layer and porous sublayer was formed.

An increase with a higher concentration of GO/Pluronic F-68 (>4 wt.%), the sublayer gradually changed into a dense sponge-like structure and the finger-like structure of the support layer displayed larger holes and extended to the bottom of the membrane. This increase indicates a delay in liquid–liquid demixing process and an acceleration in solid–liquid demixing.

In the presence of GO/Pluronic F-68 additive, the interaction between polymer and solvent molecules decreases, so that solvent molecules can diffuse more easily from the polymer matrix into coagulant. Thus, surface pore size and porosity of the impregnated membrane with GO/Pluronic F-68 additive can be larger than the neat PPF membrane. It's clear that an increase with a higher concentration of this additive (>4 wt.%), significant agglomeration takes place.

The Effect of exposure time on membrane morphology was illustrated in Fig. 4. Results show that by increasing the exposure time up to 20 min, the structure of the membrane changed from an asymmetrical structure to a symmetrical structure with the cellular structure. At zero time, the membrane structure may not change significantly during the VIPS step and the phase inversion occurs mainly by NIPS step and no VIPS occurred. The resulting morphology is similar to typical morphologies obtained by the dense layer and finger-like macrovoids.

At the time of 10 min, the mechanism of the phase inversion is a combination of VIPS and NIPS. So the structure of membranes is a combination of dense layer and finger-like macrovoids with sponge-like pores.

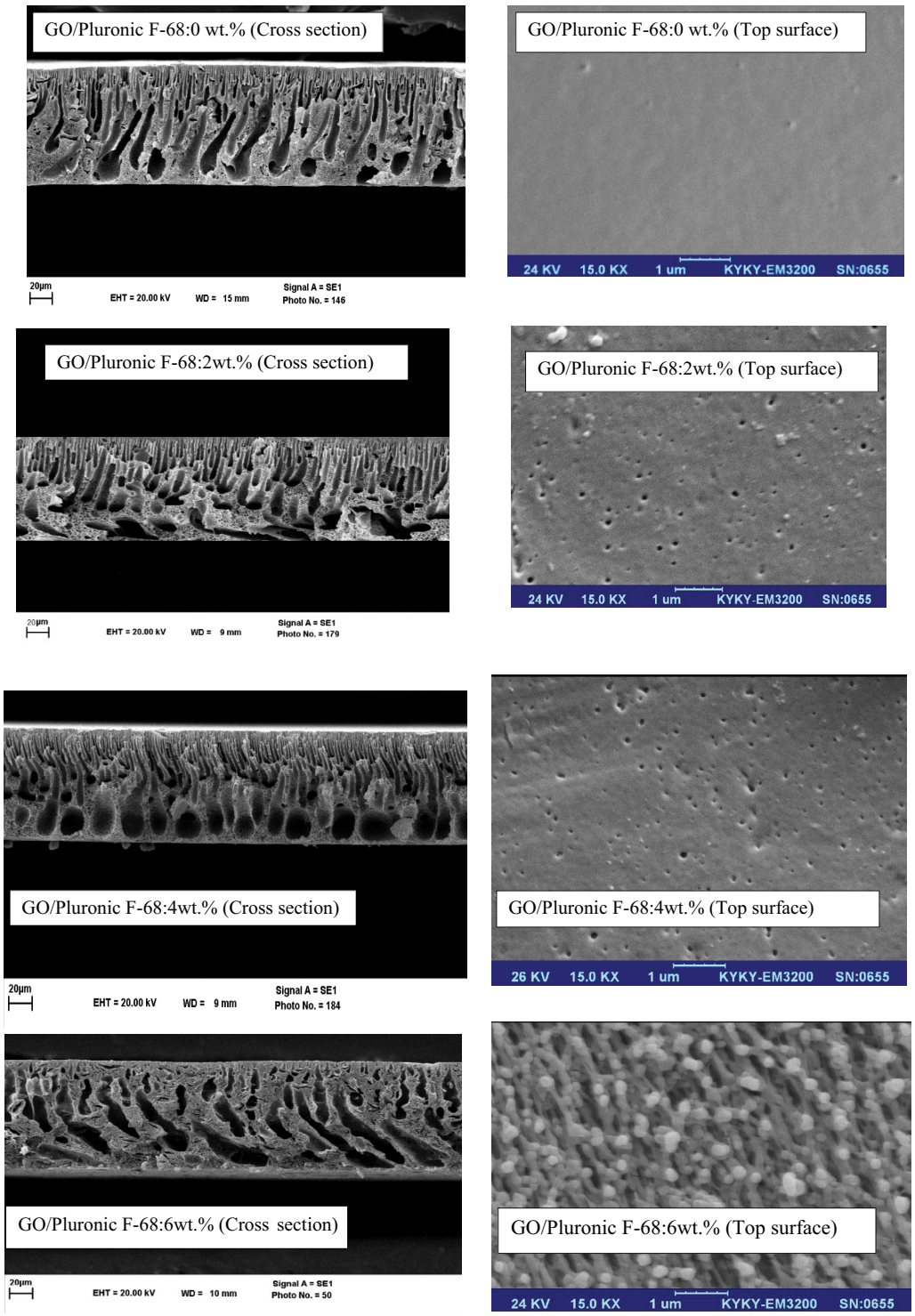

Fig. 3. SEM images of the PPF membranes modified with different concentrations of GO/Pluronic F-68 additive (exposure time: 0 min).

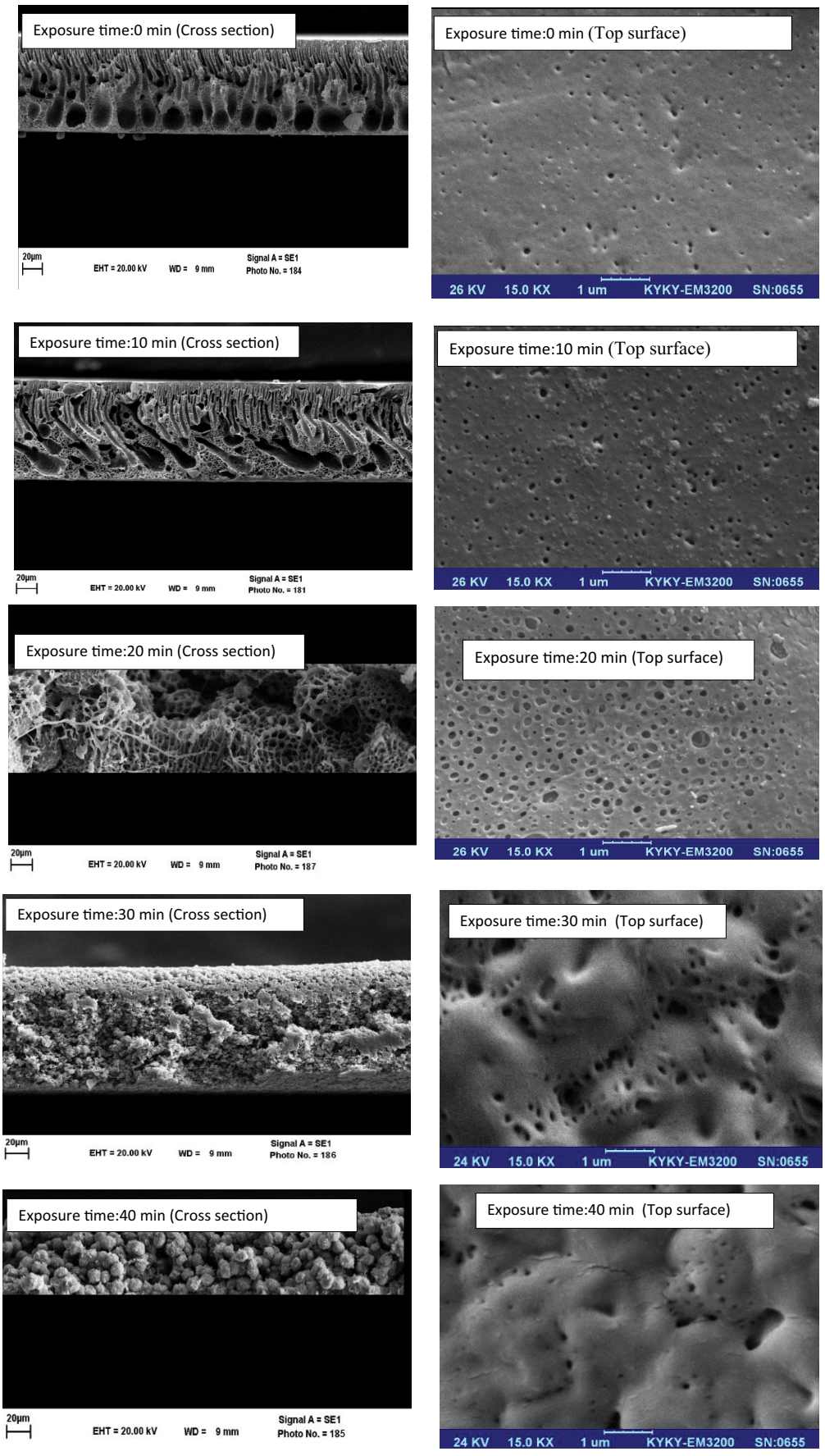

Fig. 4. SEM images of the PPF membranes prepared at different vapor exposure times (Pluronic F-68/GO: 4 wt.%).

At the time of 20 min, the mechanism of membrane formation is the VIPS process. Regarding the amorphous nature of the PPF polymer, the membrane morphology is the cellular-like structure due to the coarsening of the polymer-lean phase at the late stage of phase separation.

Also, by increasing the exposure time up to 20 min, the surface porosity was increased. However, this increase is not observed at further exposure of time. When the forming membrane was in contact with water vapor for a fixed period of time prior to the immersion in the water bath, the non-solvent vapors gradually interacted with the cast dope solution and penetrated it. So the phase separation process is mainly influenced by the vapor-induced time, which determines the content of adsorbed non-solvent. At higher exposure time (more than 20 min), wetting is prevented by air pockets trapped between the polymer and liquid phases. So with an increase in exposure time (>20 min), no further increase in surface porosity was seen.

4.2.3. Membrane porosity

The overall porosity information of prepared membranes is presented in Fig. 5. This result reveals that GO/Pluronic F-68 modified membranes offer the greater void capacity to a higher degree compared with neat PPF membrane. This is attributed to the presence of additives and their effect on phase inversion kinetic, that is, the rate of membrane precipitation during replacement of solvent and non-solvent. An increase in porosity up to 77.6% is also seen with increasing exposure time up to 20 min which is due to the expansion of the cellular structure throughout the membrane by increasing exposure time.

4.2.4. Contact angle measurement

Since PPF is a hydrophobic polymer, its hydrophobicity can be reduced significantly by adding of hydrophilic compounds. Fig. 6 illustrates the results of this measurement. As shown in Fig. 6, generally modification with GO/Pluronic F-68 is a useful method for increasing PPF membrane hydrophilicity. As can be seen, an increase in the level of hydrophilicity was found upon increasing GO/Pluronic F-68 loading from 0 to 4 wt.%. Also, it is observed that the contact angle is decreased by increasing the exposure time up to 20 min due to the high porosity of membranes than others (Fig. 7).

4.2.5. Dynamic wetting

The results of the water adsorption tests reveal the dynamic wetting behavior of the prepared membranes. The membrane shows very low adsorption before the addition of GO/Pluronic F-68, as shown in Fig. 8. When the sample is immersed into water, the effect of buoyancy of water pushes the materials upwards since the surface contact angle is almost 83°. This observation confirms the hydrophobic behavior of the PPF membrane. It can be seen from Fig. 7 that the adsorption curve of the modified porous membrane (Pluronic F-68/GO: 4 wt.%, exposure time: 30 min) displays a contrary evolution to that of the unmodified membrane. The Pluronic F-68/GO addition considerably improves the water adsorption properties of the PPF membrane due to the lower contact angles.

4.2.6. Mechanical stability measurement

4.2.6.1. Effect of GO/Pluronic F-68 content

In order to improve the mechanical properties of PPF membranes, blending with GO/Pluronic F-68 was followed. Table 1 shows the effect of GO/Pluronic F-68 addition on PPF membranes on essential mechanical properties. As can be seen the tensile modulus and strength sequentially enhanced with increasing the GO/Pluronic F-68 concentration (wt.%) up to certain values. Excessive addition of GO/Pluronic F-68 more than a certain concentration is leading to an insignificant increase in the membrane's tensile strength and Young's modulus.

The non-covalent functionalization of GO has an effective role in homogeneous dispersion in the PPF matrix. So interfacial adhesion between GO particles and polymer matrix can be improved. Additionally, the intermolecular forces between the polymeric chains and the GO dispersed uniformly in polymer causes the restriction of free motion of polymeric chains.

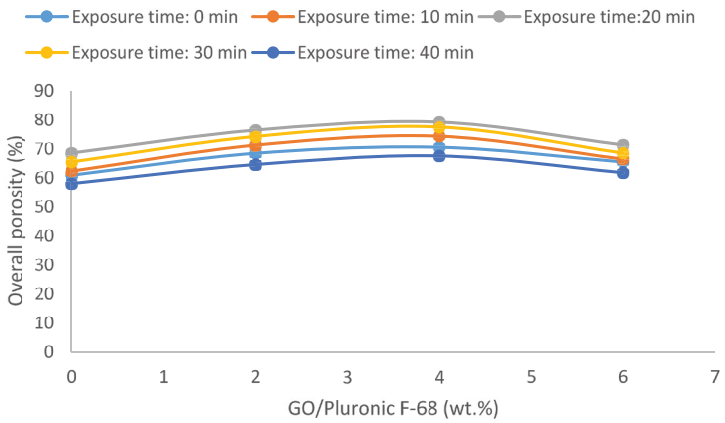

Fig. 5. Overall porosity evaluation of prepared membranes.

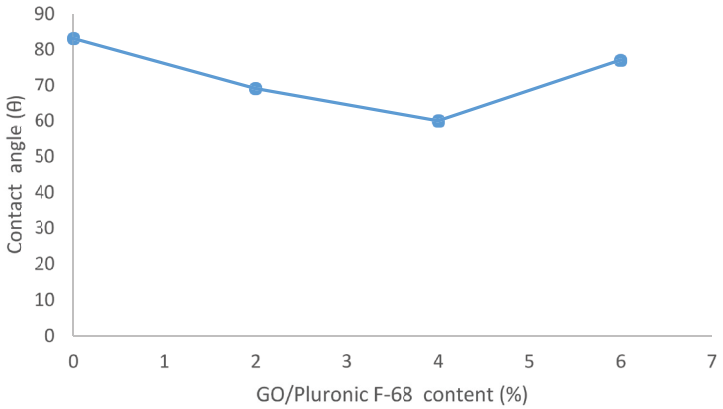

Fig. 6. Contact angle of the prepared membranes (exposure time: 0 min).

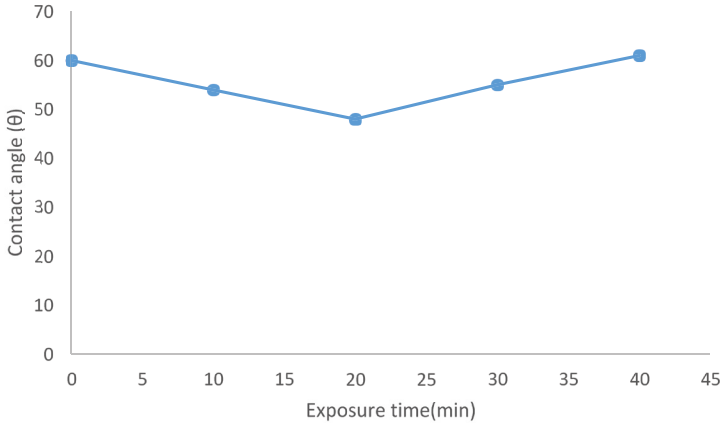

Fig. 7. Contact angle of the prepared membranes (GO/Pluronic F-68 content: 4 wt.%).

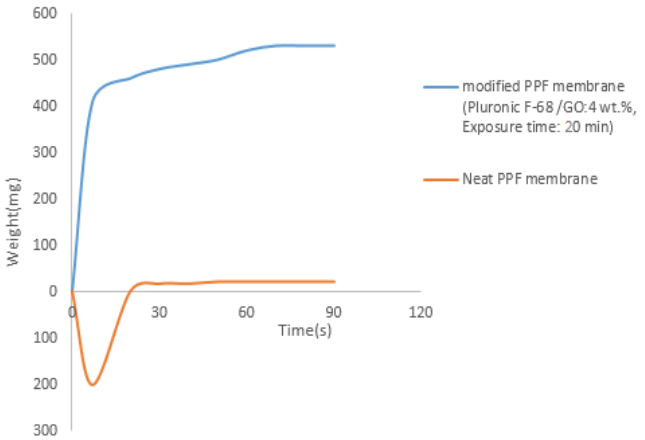

Fig. 8. Dynamic water adsorption of PPF membrane before and after modification.

The lower mechanical properties of the reinforced membranes at higher concentration of GO/Pluronic F-68 (more than 4 wt.%) compared to another one may be attributed to high porosity and large cavities that occur in the membrane structure.

4.2.6.2. Effect of exposure time

As the SEM results showed, exposure time plays an effective role in membrane morphology. So this parameter enables to adjustment the mechanical stability of the membrane. According to SEM results, the morphology of the membranes tends to cellular structure when the exposure time increases from 0 to 20 min. Generally, by the formation of symmetric cellular structures the mechanical properties strengthened than the asymmetric structure of the dense skin layer with finger-like macrovoids obtained from the NIPS process (zero exposure time). Also, the mechanical properties of modified membranes decreased with increasing exposure time from 20 to 40 min. This behavior may be attributed to coalesces of GO/Pluronic F-68 and higher crosslinking density results in crystalline wrecking.

4.2.7. Measurement of the MWCO and average pore size of the prepared membranes

The MWCO results for all the membranes were determined individually based on the percentage rejection data of PEG and dextran (Fig. 9 and Table 2). As observed, the MWCO increases by GO/Pluronic F-68 concentration up to 4 wt.%. Also, it is observed that the MWCO is

Table 1
Mechanical properties of the PPF membranes modified with GO/Pluronic F-68

Exposure time (min)	Pluronic F-68/GO content (wt.%)	Tensile strength (MPa)	Young's modulus (MPa)	Elongation at break (mm)
0	0	2.7	72	1.93
	2	3.5	82	2.36
	4	4.2	88	2.3
	6	3	73	1.1
10	0	3.3	74	2.1
	2	3.7	85	2.41
	4	4.6	91	2.5
	6	4	88	1.93
20	0	3.7	76	2.3
	2	4.8	88	2. 6
	4	5	94	2.3
	6	4.2	90	2.1
30	0	3.1	73	1.95
	2	3.7	83	2.61
	4	4.5	89	2.38
	6	3.4	76	1.45
40	0	2.9	71	1.96
	2	3.6	84	2.4
	4	4.3	90	2.36
	6	3.2	75	1.27

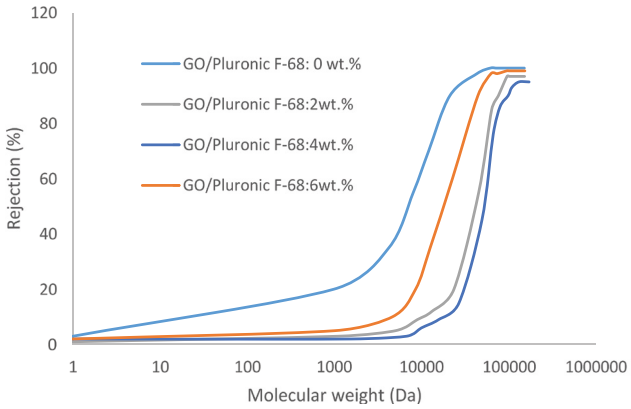

Fig. 9. Rejection rate curve of different molecular weights of solute for prepared membranes (exposure time: 20 min).

increased by increasing the exposure time up to 20 min due to the high porosity of membranes than others. Generally, a highly porous membrane offers lower solute rejection and hence higher MWCO. Therefore, at the 4 wt.% concentration of GO/Pluronic F-68 with an exposure time of 20 min, a more porous membrane with a higher MWCO of 97.8 kDa was obtained. However, for neat membrane (exposure time of 0 min), the lowest MWCO of 29.2 kDa was obtained due to its dense and thicker membrane morphology.

Table 2
MWCO and average pore size of prepared membranes

Exposure time (min)	Pluronic F-68/GO content (wt.%)	MWCO (kDa)	Average pore size (nm)
0	0	29.2	5.13
	2	32.6	5.46
	4	44.3	6.47
	6	30	5.21
10	0	32.5	5.45
	2	38.6	6
	4	65.4	8.049
	6	34.8	5.66
20	0	36	5.77
	2	75.6	8.72
	4	97.8	10.07
	6	44	6.45
30	0	34	5.59
	2	40.2	6.13
	4	77.3	8.83
	6	38.3	5.97
40	0	28.4	5.05
	2	30.3	5.24
	4	40.7	6.18
	6	28.1	5.02

The unmodified membrane (exposure time: 0 min) has the smallest average pore size of about 5.13 nm on the membrane surface, as tabulated in Table 2. The trend of the average pore size is similar to that of MWCO. So, the prepared membrane with GO/Pluronic F-68 concentration of 4 wt.% (exposure time: 20 min) has a higher average pore size than others. The increased average pore sizes of the resultant blend membranes up to 4 wt.% were due to the increasing nature of immiscible phase behavior of blend, attributed to low molecular attractive forces between the blend components, and as a result produced membranes with open (more extensive) pores size.

4.3. Anti-bacteria and anti-biofouling performance

Figs. 10 and 11 show some typical results indicating the anti-bacteria and anti-biofouling of prepared membrane performance. The high reduction in bacteria density can be observed around modified membrane concerning another one. Hydrophilic modification of PPF by Pluronic F-68/GO can decrease bacterial proliferation. Since the bacteria tend to grow on hydrophobic surfaces, so hydrophilic surfaces may prohibit bacterial proliferation.

Anti-biofouling behavior of the neat and modified membranes evaluated after immersing in *E. coli* suspension. The anti-biofouling performance of membranes was studied by CFU, determining on neat and modified membrane specimens. Fig. 11 illustrates the CFU results of *E. coli*. As can be seen, a highly significant decrease in CFU is observed in the presence of modified membranes compared to the unmodified ones. Also, the SEM analysis was conducted to investigate further the anti-biofouling behavior of the membrane samples (Fig. 12). The neat PPF membrane surface was covered by bacterial congestion, while the coverage of modified membrane surfaces was significantly lower with several isolated bacterial colonies. In fact, by forming the hydration layer near the surface resulting in hydrophilicity of the membrane, the energy barrier is created. So the bacteria and pollutants kept away from approaching the membrane surface.

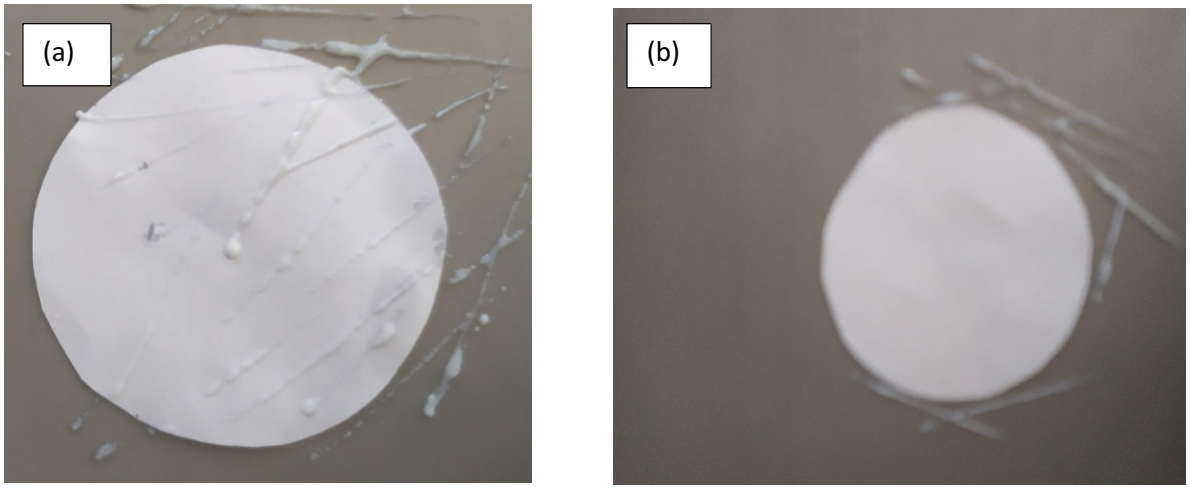

Fig. 10. Images of bacteria growth on (a) neat PPF and (b) PPF/Pluronic F-68/GO (4 wt.%) membranes.

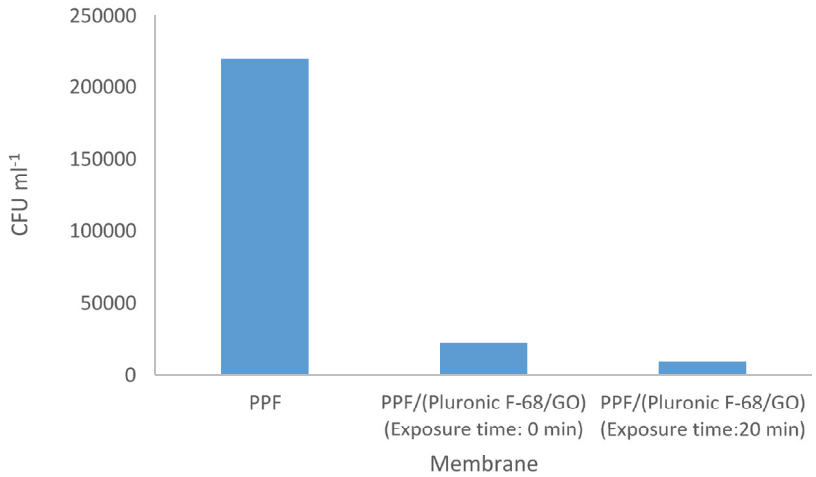

Fig. 11. CFU results of *Escherichia coli* on modified and unmodified membranes.

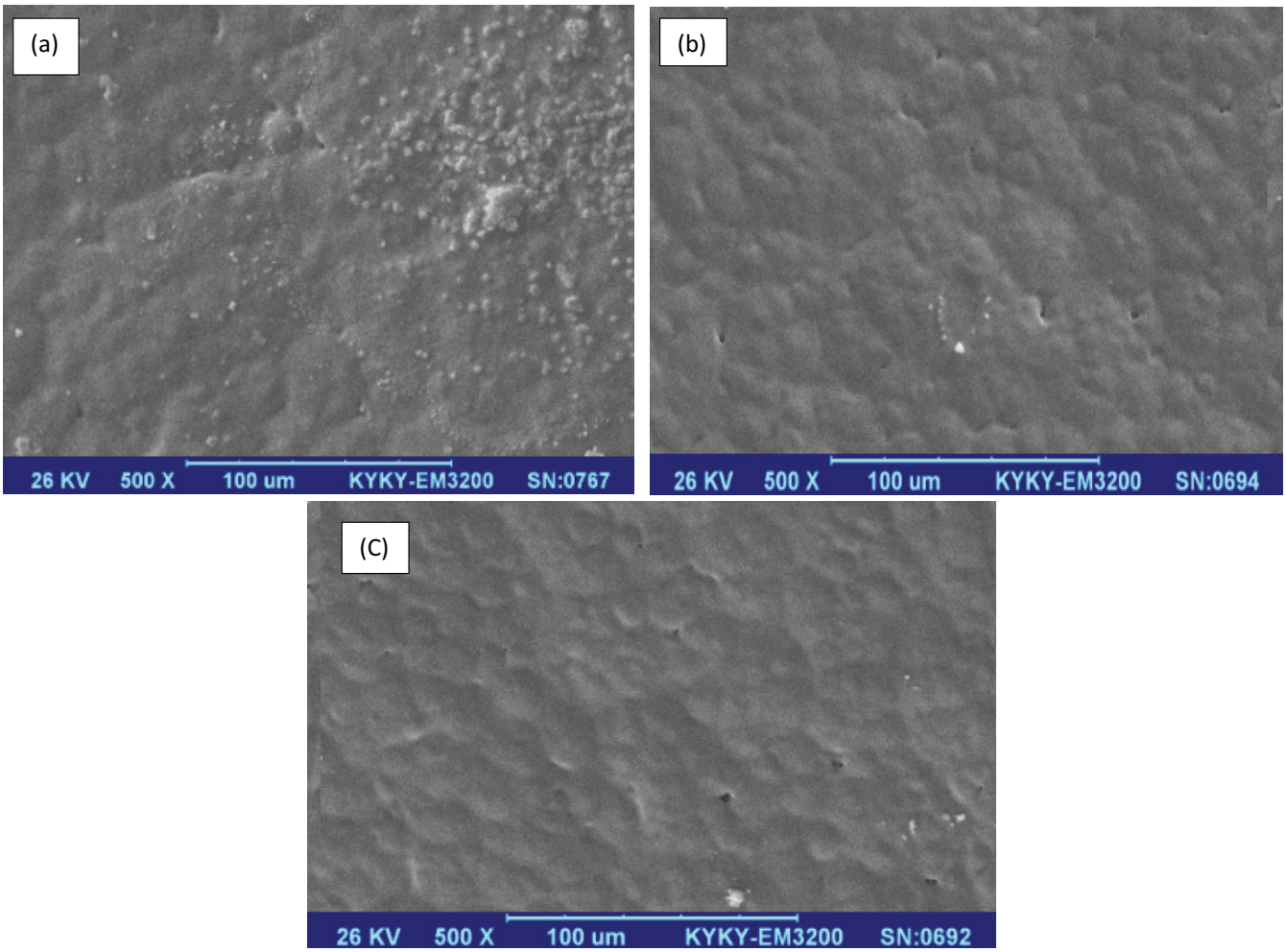

Fig. 12. SEM image of membranes surface after immersing in *Escherichia coli* suspension, (a) neat PPF membrane, (b) PPF/Pluronic F-68/GO (4 wt.%) (exposure time: 0 min), and (c) PPF/Pluronic F-68/GO (4 wt.%) (exposure time: 20 min).

It is noticeable that additive role is predominant in the investigation of anti-bacteria and anti-fulling behavior, so exposure time has little role in anti-bacteria and anti-fulling properties.

4.4. Membrane permeability and rejection performance

The results of pure water permeability of prepared membranes are presented in Fig. 13. As shown, the prepared membranes with modification by Pluronic F-68/GO present higher pure water permeability than the neat PPF membrane. This value enhances by considering Pluronic F-68/GO up to 45%. After adhesion of Pluronic F-68/GO additive up to 4 wt.% in the casting solution, the abundant oxygenate functional groups increased in the membrane surface that may lead to more hydrogen bonds between water molecules and the surface of the membrane. Therefore, the tendency to absorb water increases. By increasing the exposure time Up to 20 min, the prepared membrane presents higher pure water permeability in comparison with those that were not exposed to vapor.

The influences of the Pluronic F-68/GO contents and vapor exposure time s on the permeation flux are shown in Fig. 14. Obviously, the permeation flux increases with the introduction of additive. As can be seen in Fig. 14, the permeate flux of all membranes reduces drastically with time, which is rapid during the first 10 min and then followed by a more gradual decline until becomes constant. This behavior refers to concentration polarization and fouling of the membranes. The trend of the wastewater permeation flux is almost similar to that of pure water flux. So, the prepared membranes exposed to vapor up to 20 min have higher fluxes than others.

When the exposure time increased up to 20 min, the membrane structure changed from asymmetrical to the symmetrical and cellular structure by the coarsening of the polymer lean phase, at the late stage of phase inversion. Therefore, the size of the cell increased, resulting in a pore size enlargement. Thus, higher membrane permeability could be recorded. After that, by more increasing, the coalescence of the polymer-rich phase results in a decrease the interconnectivity of pores.so there is no inter-connection between the pores. Consequently, a decrease in the membrane permeability occurs.

The COD, TDS, and turbidity rejection results for unmodified and modified PPF membranes are shown in Table 3.

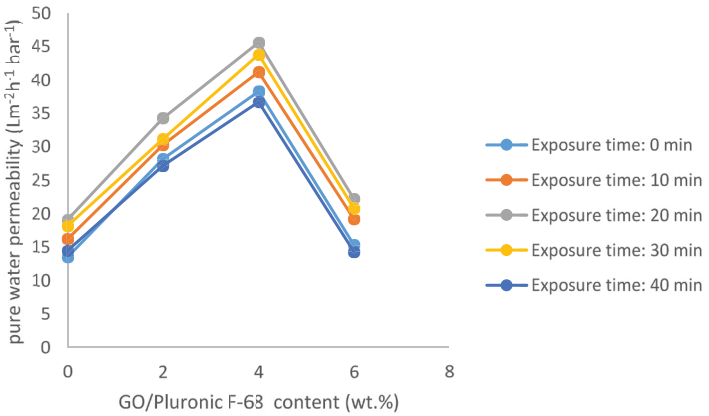

Fig. 13. Pure water permeability of prepared modified PPF membranes.

Since the surface of the neat PPF membrane is hydrophobic, a relatively high amount of pollutant adsorbed on the surface irreversibly and leads to cake layer formation. So, a decrease in porosity and pore size of membrane surface occurs. After deposition of Pluronic F-68/GO on the membrane surface, the hydrophilicity of the membrane surface is improved and free water fraction is increased. Consequently, the irreversible pollutant adsorption on the membrane surface is reduced. As a result, the COD rejection ratio of the modified membrane is higher than that of the corresponding neat PPF membrane and reaches up to 94%.

The TDS rejection result is also similar to COD rejection. It means that TDS rejection is increased by adding Pluronic F-68/GO additive to polymer matrix. As shown in Table 3, in the presence or absence of Pluronic F-68/GO additive, the turbidity rejection is above 90%. The results indicate that these membranes can be solely sufficient to reduce turbidity of the wastewater. Therefore, adding the additives does not have a considerable effect on turbidity rejection. At a higher exposure time which forms low porous structures (granular structure), the resistance against the transmission of wastewater increases. Obviously, with increasing in resistance against the transmission, the selectivity of membranes increases.

Furthermore, the anti-biofouling performance of membranes shows that the Pluronic F-68/GO modified membranes have anti-biofouling properties, since some of the pollutants are biological, so they are expected to perform

Table 3
Evaluation of PPF membranes modified with Pluronic F-68/GO

Exposure time (min)	Pluronic F-68/GO content (wt.%)	Average value of COD rejection in twice replicates	Average value of TDS rejection in twice replicates	Average value of turbidity rejection in twice replicates
0	0	42	32	90
	2	69	54	91.1
	4	80	73	92
	6	85	78	92.5
10	0	45	35	91.9
	2	71	51	92.1
	4	83	71	93
	6	87	81	93.2
20	0	46	40	92
	2	74	57	92.4
	4	85	77	93
	6	89	85	93.5
30	0	50	42	93
	2	77	59	93.2
	4	87	80	93.4
	6	92	88	93.8
40	0	53	46	93
	2	86	69	93.5
	4	91	84	94
	6	94	90	94

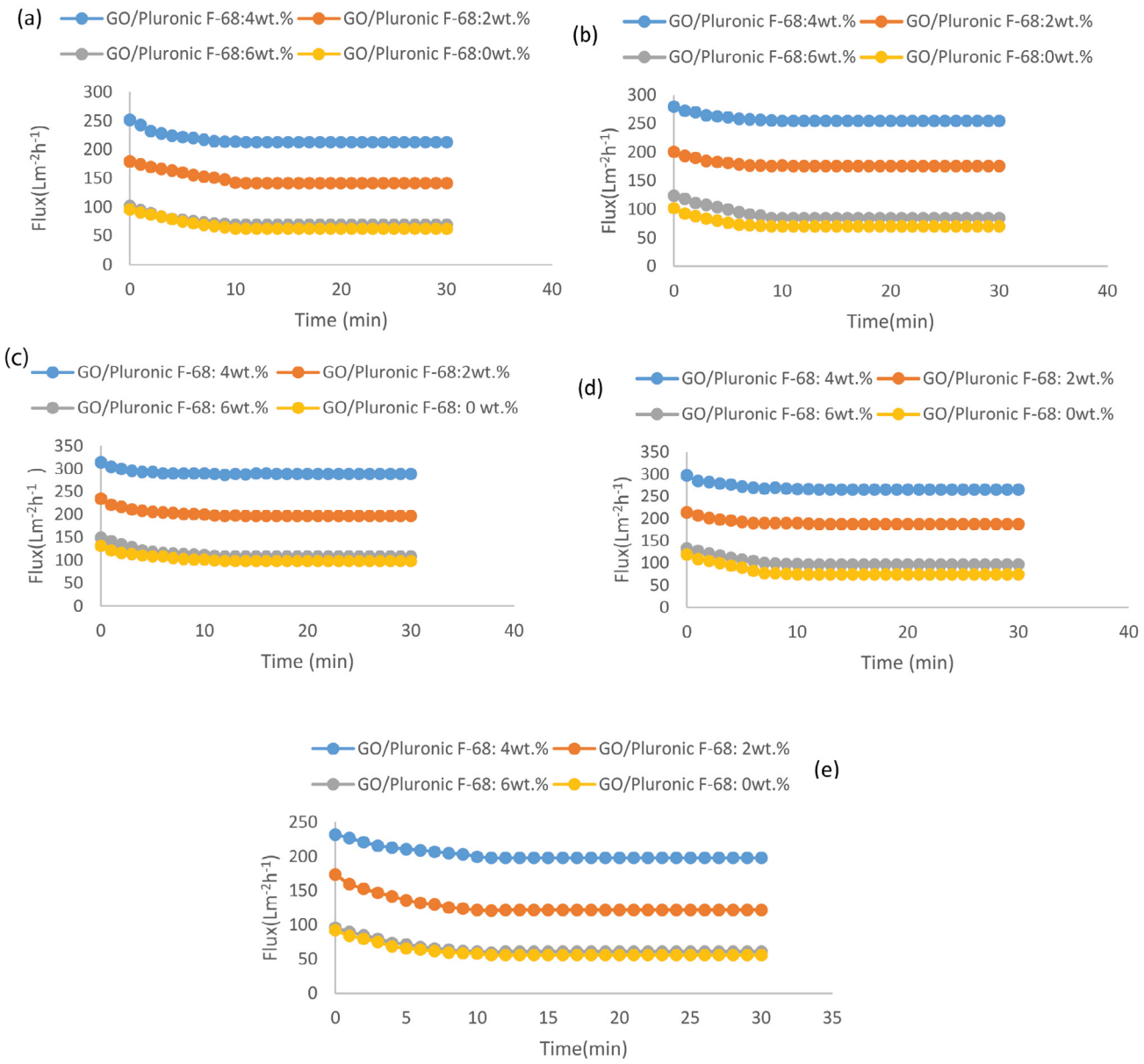

Fig. 14. Permeate flux of ceramic factory wastewater through the prepared membranes, (a) exposure time: 0 min, (b) exposure time: 10 min, (c) exposure time: 20 min, (d) exposure time: 30 min, and (e) exposure time: 40 min.

well in rejections. Generally compared to other ultrafiltration membranes, the Pluronic F-68/GO modified membranes had better performance [35–37].

5. Conclusion

In this paper, the propylene fumarate membranes were modified with Pluronic F-68/GO additive. These membranes were prepared via the VIPS process. In terms of effective parameters in membrane formation, Pluronic F-68/GO concentration and vapor exposure time were evaluated. Membrane morphology, mechanical properties as well as membrane performance are presented. PPF membrane hydrophilicity was changed by adding Pluronic F-68/GO to the casting solution (up to 4 wt.%), and the hydrophobic interaction between the membrane surface and pollutants is decreasing. Different trends and morphologies have been observed at various exposure times. At lower times (<20 min), there is a finger-like structure that is formed. At higher times (>20 min), cell-like and granular structures tend to form. It was revealed that the mechanical properties of the (Pluronic F-68/GO)/PPF membranes increase with increasing the Pluronic F-68/GO content up to 4 wt.%. The lower mechanical properties of the reinforced membranes at higher concentration of GO/Pluronic F-68 (more than 4 wt.%) compared to another one may be

attributed to high porosity and large cavities that occur in the membrane structure. Also, by the formation of symmetric cellular structures at higher exposure times, the mechanical properties strengthened than the asymmetric structure of the dense skin layer with finger-like macrovoids obtained from the NIPS process (zero exposure time). The experimental results generally showed that the addition of GO/Pluronic F-68 also increased the MWCO and average pore size of Pluronic F-68/GO blend membranes. The modified PPF membranes displayed higher resistance to biofouling than the unmodified membranes. SEM analysis revealed that less bacterial coverage and growth occurred on the modified PPF membrane surfaces. These membranes present higher pure water permeability in comparison with the neat PPF membrane. It is important to note that the membranes modified with Pluronic F-68/GO have a high ability to reduction of wastewater pollution indices in comparison with the neat PPF membrane.

References

[1] N. Ismail, A. Venault, J.-P. Mikkola, D. Bouyer, E. Drioli, N. Tavajohi, H. Kiadeh, Investigating the potential of membranes formed by the vapor induced phase separation process, J. Membr. Sci., 597 (2019) 117601, doi: 10.1016/j.memsci.2019.117601.

[2] M. Omidvar, S.M. Mousavi, M. Soltanieh, A.A. Safekordi, Preparation and characterization of poly (ethersulfone) nanofiltration membranes for amoxicillin removal from contaminated water, J. Environ. Health Sci. Eng., 12 (2014) 2–9.

[3] N.I.M. Nawi, H.M. Chean, N. Shamsuddin, M.R. Bilad, T. Narkkun, K. Faungnawakij, A.L. Khan, Development of hydrophilic PVDF membrane using vapour induced phase separation method for produced water treatment, Membranes, 10 (2020) 121, doi: 10.3390/membranes10060121.

[4] M. Khajouei, M. Najafi, S.A. Jafari, Development of ultrafiltration membrane via in-situ grafting of nano-GO/PSF with anti-biofouling properties, Chem. Eng. Res. Des., 142 (2019) 34–43.

[5] A.M. Diez-Pascual, Tissue engineering bionanocomposites based on poly(propylene fumarate), Polymers, 9 (2017) 260, doi: 10.3390/polym9070260.

[6] F.K. Kasper, K. Tanahashi, J.P. Fisher, A.G. Mikos, Synthesis of poly(propylene fumarate), Nat. Protoc., 4 (2009) 518–525.

[7] S. Bano, A. Mahmood, S.-J. Kim, K.-H. Lee, Graphene oxide modified polyamide nanofiltration membrane with improved flux and antifouling properties, J. Mater. Chem. A, 3 (2015) 2065–2071.

[8] A. Venault, A.J. Jumao-as-Leyba, Z.-R. Yang, S. Carretier, Y. Chang, Formation mechanisms of low-biofouling PVDF/F127 membranes prepared by VIPS process, J. Taiwan Inst. Chem. Eng., 62 (2016) 297–306.

[9] Q. Shi, Y. Su, X. Ning, W. Chen, J. Peng, Z. Jiang, Graft polymerization of methacrylic acid onto polyethersulfone for potential pH-responsive membrane materials, J. Membr. Sci., 347 (2010) 62–68.

[10] B. Liu, C. Chen, C.J. Zhang, Y. Chen, Low-cost antifouling PVC ultrafiltration membrane fabrication with Pluronic F127: effect of additives on properties and performances, Desalination, 307 (2012) 22–33.

[11] Y. Mansourpanah, H. Shahebrahimi, E. Kolvari, PEG-modified GO nanosheets, a desired additive to increasethe rejection and antifouling characteristics of polyamide thinlayer membranes, Chem. Eng. Res. Des., 104 (2015) 530–540.

[12] H. Matsuyama, T. Maki, M. Teramoto, K. Kobayashi, Effect of PVP additive on porous polysulfone membrane formation by immersion precipitation method, Sep. Sci. Technol., 38 (2008) 3449–3458.

[13] J.S. Louie, I. Pinnau, I. Ciobanu, K.P. Ishida, A. Ng, M. Reinhard, Effects of polyether–polyamide block copolymer coating on performance and fouling of reverse osmosis membranes, J. Membr. Sci., 280 (2006) 762–770.

[14] H. Ju, B.D. McCloskey, A.C. Sagle, Y.H. Wu, V.A. Kusuma, B.D. Freeman, Crosslinked poly(ethylene oxide) fouling resistant coating materials for oil/water separation, J. Membr. Sci., 307 (2008) 260–267.

[15] S. Yu, G. Yao, B. Dong, H. Zhu, X. Peng, J. Liu, M. Liu, C. Gao, Improving fouling resistance of thin-film composite polyamide reverse osmosis membrane by coating natural hydrophilic polymer sericin, Sep. Purif. Technol., 118 (2013) 285–293.

[16] A.O. Rashed, A.M.K. Esawi, A.R. Ramadan, Novel polysulfone/carbon nanotube-polyamide thin film nanocomposite membranes with improved water flux for forward osmosis desalination, ACS Omega, 5 (2020) 14427–14436.

[17] E. Igbinigun, Y. Fennell, R. Malaisamy, K.L. Jones, V. Morris, Graphene oxide functionalized polyethersulfone membrane to reduce organic fouling, J. Membr. Sci., 514 (2016) 518–526.

[18] F. Kouhestani, M.A. Torangi, A. Motavalizadehkakhky, R. Karazhyan, R. Zhiani, Enhancement strategy of polyethersulfone (PES) membrane by introducing pluronic F127/graphene oxide and phytic acid/graphene oxide blended additives: preparation, characterization and wastewater filtration assessment, Desal. Water Treat., 171 (2019) 44–56.

[19] R.K. Joshi, S. Alwarappan, M. Yoshimura, V. Sahajwalla, Y. Nishina, Graphene oxide: the new membrane material, Appl. Mater. Today, 1 (2015) 1–12.

[20] H. Ahmad, M. Fan, D. Hui, Graphene oxide incorporated functional materials: a review, Composites, Part B, 145 (2018) 270–280.

[21] S. Xia, M. Ni, Preparation of poly (vinylidene fluoride) membranes with graphene oxide addition for natural organic matter removal, J. Membr. Sci., 473 (2015) 54–62.

[22] R. Li, L. Liu, Y. Zhang, F. Yang, Preparation of a nano-MnO_2 surface-modified reduced graphene oxide/PVDF flat sheet membrane for adsorptive removal of aqueous Ni(II), RSC Adv., 6 (2016) 20542–20550.

[23] X.-F. Sun, J. Qin, P.-F. Xia, B.-B. Guo, C.-M. Yang, C. Song, S.-G. Wang, Graphene oxide–silver nanoparticle membrane for biofouling control and water purification, Chem. Eng. J., 281 (2015) 53–59.

[24] A. Gosai, K.R. Khondakar, X. Ma, M.A. Ali, Application of functionalized graphene oxide based biosensors for health monitoring: simple graphene derivatives to 3D printed platforms, Biosensors, 11 (2021) 384–404.

[25] C. Zhang, F. Wang, Z. Jiang, J. Lan, L. Zhao, P. Si, Effect of graphene oxide on the mechanical, tribological, and biological properties of sintered 3Y–ZrO_2/GO composite ceramics for dental implants, Ceram. Int., 47 (2021) 6940–6946.

[26] J.M. Luque-Alled, A. Abdel-Karim, M. Alberto, S. Leaper, M. Perez-Page, K. Huang, A. Vijayaraghavan, A.S. El-Kalliny, S.M. Holmes, P. Gorgojo, Polyethersulfone membranes: from ultrafiltration to nanofiltration via the incorporation of APTS functionalized-graphene oxide, Sep. Purif. Technol., 230 (2020) 115836, doi: 10.1016/j.seppur.2019.115836.

[27] W. Wu, Y. Shi, G. Liu, X. Fan, Y. Yu, Recent development of graphene oxide based forward osmosis membrane for water treatment: a critical review, Desalination, 491 (2020) 114452, doi: 10.1016/j.desal.2020.114452.

[28] X. Tang, W. Li, Z. Yu, Enhanced thermal stability in graphene oxide covalently functionalized with 2-amino-4,6-didodecylamino-1,3,5-triazine, Carbon, 49 (2011) 1258–1265.

[29] A.R. Rico, M. Cucchiarini, PEO-PPO-PEO tri-block copolymers for gene delivery applications in human regenerative medicine—an overview, Int. J. Mol. Sci., 19 (2018) 775, doi: 10.3390/ijms19030775.

[30] M. Ebrahimpour, A.A. Safekordi, S.M. Mousavi, A. Heydarinasab, Modification strategy of biodegradable poly (butylene succinate) (PBS) membrane by introducing Al_2O_3 nanoparticles: preparation, characterization and wastewater treatment, Desal. Water Treat., 79 (2017) 19–29.

[31] F. Shen, X. Lu, X. Bian, L. Shi, Preparation and hydrophilicity study of poly(vinyl butyral)-based ultrafiltration membranes, J. Membr. Sci., 265 (2005) 74–84.
[32] M. Khayet, T. Matsuura, Determination of surface and bulk pore sizes of flat-sheet and hollow-fiber membranes by atomic force microscopy, gas permeation and solute transport, Desalination, 158 (2003) 57–64.
[33] S.R. Panda, S. De, Effects of polymer molecular weight, concentration, and role of polyethylene glycol as additive on polyacrylonitrile homopolymer membranes, Polym. Eng. Sci., 54 (2014) 2375–2391.
[34] J.H. Li, Y.Y. Xu, L.P. Zhu, J.H. Wang, C.H. Du, Fabrication and characterization of a novel TiO_2 nanoparticle self-assembly membrane with improved fouling resistance, J. Membr. Sci., 326 (2009) 659–666.
[35] H.T. Dang, R.M. Narbaitz, T. Matsuura, D. Rana, Performance Evaluation of Commercial and Newly-Developed Ultrafiltration Membranes: Surface Analysis and Fouling Tests, American Water Works Association – AWWA Annual Conference and Exposition, ACE, 2007, pp. 602–616.
[36] R.M. Narbaitz, D. Rana, H.T. Dang, J. Morrissette, T. Matsuura, S.Y. Jasim, S. Tabe, P. Yang, Field Testing of Modified CA Membranes to Remove PPCP from Drinking Water, AMTA/ AWWA Membrane Technology Conference and Exposition, 2013, pp. 107–123.
[37] D. Rana, T. Matsuura, State of the art reviews in membrane science and research, J. Membr. Sci. Res., 3 (2017) 118–119.